6th European Conference on Computational Mechanics (ECCM 6)
7th European Conference on Computational Fluid Dynamics (ECFD 7)
11-15 June 2018, Glasgow, UK

A FICTITIOUS DOMAIN METHOD WITH HIGHER-ORDER ACCURATE INTEGRATION IN CUT ELEMENTS

T.P. Fries[1], S. Omerović[1], D. Schöllhammer[1] and J. Stanford[1]

[1] Institute of Structural Analysis
Graz University of Technology
Lessingstr. 25/II, 8010 Graz, Austria
www.ifb.tugraz.at
fries@tugraz.at

Key words: higher-order FEM, p-FEM, level-set method, fictitious domain method, embedded domain method, immersed boundary method

Abstract. A higher-order accurate fictitious domain method (FDM) is proposed based on higher-order background meshes and multiple level-set functions for the definition of the domain of interest. Elements cut by the zero-level sets are decomposed into higher-order sub-elements conforming to the implied boundaries. Integration points are placed in those sub-elements belonging to the domain. Boundary conditions are enforced using Lagrange multplier or penalty methods. Ill-conditioned systems of equations are avoided using negligible material parameters in the void regions. The resulting FDM is compared to the conformal decomposition FEM (CDFEM) as both methods share the decomposition of cut elements. Higher-order convergence rates are obtained with for both methods.

1 INTRODUCTION

In the context of solving boundary value problems, it is well-known that the domains of interest may be described explicitly (e.g., as in computer aided geometric design using NURBS [7, 27]) or implicitly based on the level-set method [25, 24, 31]. Herein, the level-set method is used and multiple level-set functions are employed to describe complex domains. For the analysis, a non-conforming background mesh is used as a starting point into which the domain is completely immersed. Two different procedures are then investigated: The first relies on the automatic generation of suitable conforming meshes leading to the conformal decomposition finite element method (CDFEM). The second path is to employ the elements and shape functions implied by the background mesh in the sense of a fictitious domain method (FDM). In particular, the aim is to achieve *higher-order accurate* approximations of boundary value problems, herein in the context of linear elasticity.

For both approaches, the accurate decomposition of the elements cut by the zero-level sets into higher-order sub-elements is a crucial step. This has been outlined in previous

works, e.g., in [12, 23, 11, 9, 14, 13]. In FDMs, these sub-elements are used for integration purposes only, as shape functions are generated from the background mesh. In the CDFEM, these sub-elements replace the original background elements and directly provide basis functions and degrees of freedom. For the decomposition, (i) cut background elements are identified, (ii) the positions of the zero-level sets are reconstructed by interface elements, and (iii) sub-elements are generated on both sides.

Some previous works on the CDFEM include [22] in a low-order context and [11] for higher orders. In the CDFEM, the resulting sub-elements are combined to yield a regular, conforming, higher-order mesh. For the success, adaptive refinements of the background mesh are crucial to handle complex level-set data where the decomposition may fail without refinements. To avoid ill-shaped elements, nodes of the background mesh which are too close to zero-level sets are (slightly) moved following [19, 16, 14, 11]. Once the mesh is automatically generated, a classical p-FEM analysis is conducted.

There is a rich body of literature in methods related to FDMs: the unfitted or cut finite element method [4, 5, 3, 15], finite cell method [1, 8, 26, 29, 30], Cartesian grid method [33, 34], immersed interface method [17], virtual boundary method [28], embedded domain method [20, 21] etc. The important difference between the CDFEM and FDMs is that the first uses the shape functions of the decomposed elements in the conforming mesh as the approximation basis whereas the second employs the shape functions of the original background mesh and uses the sub-elements for integration purposes only. Next to the accurate integration in cut elements, major challenges in FDMs are: The imposition of boundary conditions along the inner-element boundaries of the domain and the conditioning of the resulting system of equations. For the boundary conditions, we use Lagrange multipliers or the penalty method which are well-known approaches for enforcing general constraints. To ensure well-conditioned systems of equations, a negligible Young's modulus is prescribed in the void regions as, e.g., suggested in the finite cell method [8, 26, 30]. One may also possibly use stabilizations similar to those suggested in [4, 5, 3, 15] which, however, are beyond the scope of this work.

The paper is organized as follows: In Section 2, the concept of implicit geometry descriptions based on multiple level-set functions is outlined. The process of identifying cut elements, reconstructing the zero-level sets by interface elements, and decomposing cut elements into sub-elements is outlined which is relevant for both, the CDFEM and FDM. The CDFEM is described in Section 3 and the proposed variant of the FDM in Section 4. Numerical results are presented in Section 5 and higher-order convergence rates are achieved. Finally, the paper ends with a summary and conclusion in Section 6.

2 RECONSTRUCTION AND DECOMPOSITION

This section describes the shared starting point for the CDFEM and FDM described below and closely follows [12, 23, 11, 9, 14]. Consider a domain of interest Ω in two dimensions which is fully immersed in a background mesh composed by (possibly unstructured) higher-order Lagrange elements. The boundary of the domain is implied by the zero-contours of level-set functions $\phi_i(\boldsymbol{x})$. The level-set functions are evaluated at the nodes of the background mesh and, in between, interpolated by $\phi_i^h(\boldsymbol{x})$ based on classical finite

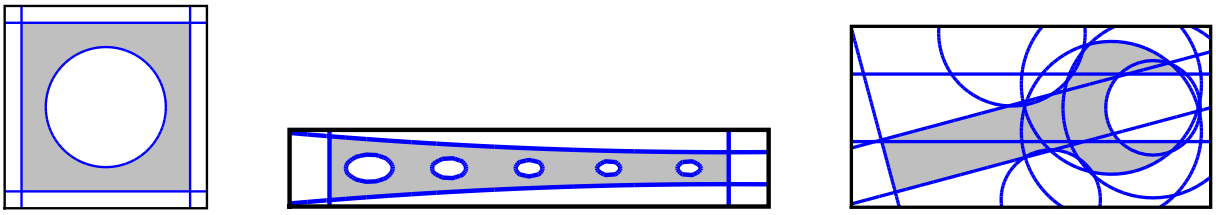

(a) plate with hole (b) cantilever beam (c) spanner

Figure 1: Zero-level sets (blue lines) in 2D and the implied geometries Ω (gray areas) of a (a) plate with hole, (b) cantilever beam, and (c) spanner.

element shape functions. The signs of the level-set functions define sub-regions in the background mesh and k level-set functions may define up to 2^k subregions. Based on the sign-combinations of the involved level-set functions, one may easily identify void regions or parts of the domain Ω. See Fig. 1 for some examples which are later considered in the numerical results. It is also seen that several level-set functions naturally imply corners and edges of the domain of interest [13, 10]. Consequently, a purely implicit description of complex geometries of practical interest is possible using multiple level-set functions.

The task is to decompose the background mesh into higher-order sub-elements which conform to the zero-level sets, i.e., to the boundary of Ω. This is done successively with respect to all level-set functions in an element-wise fashion. For each level-set function, the following steps are performed in every *reference* background element, see Fig. 2(a) and references [12, 13, 11] for further details:

1. Detection whether the element is cut by the current level-set function or not. Therefore, the nodal values are interpolated on a sample grid. The element is cut if different signs of the level-set values at the grid points are detected. For cut elements proceed with step 2, otherwise with the next element.

2. Based on the sample grid and moderately complex level-set data, determine how the zero-level set cuts the element and classify the topological cut situation. Otherwise, for complex level-set data (e.g., defining multiple, unconnected zero-level sets within the element, or zero level-sets which leave and re-enter the element), refining the background elements recovers valid situations, as discussed below.

3. Reconstruction: In the reference element, identify the zero-level set (representing parts of the boundary) and define interface elements. Therefore, element nodes are identified on the zero-level set along specified search paths for which a tailored Newton-Raphson scheme is employed. The definition of such search paths and the corresponding start values for the iteration are crucial for the success.

4. Decomposition: Decompose the reference element based on the reconstructed interface element wherefore customized mappings of sub-elements are employed depending on the topological cut situation.

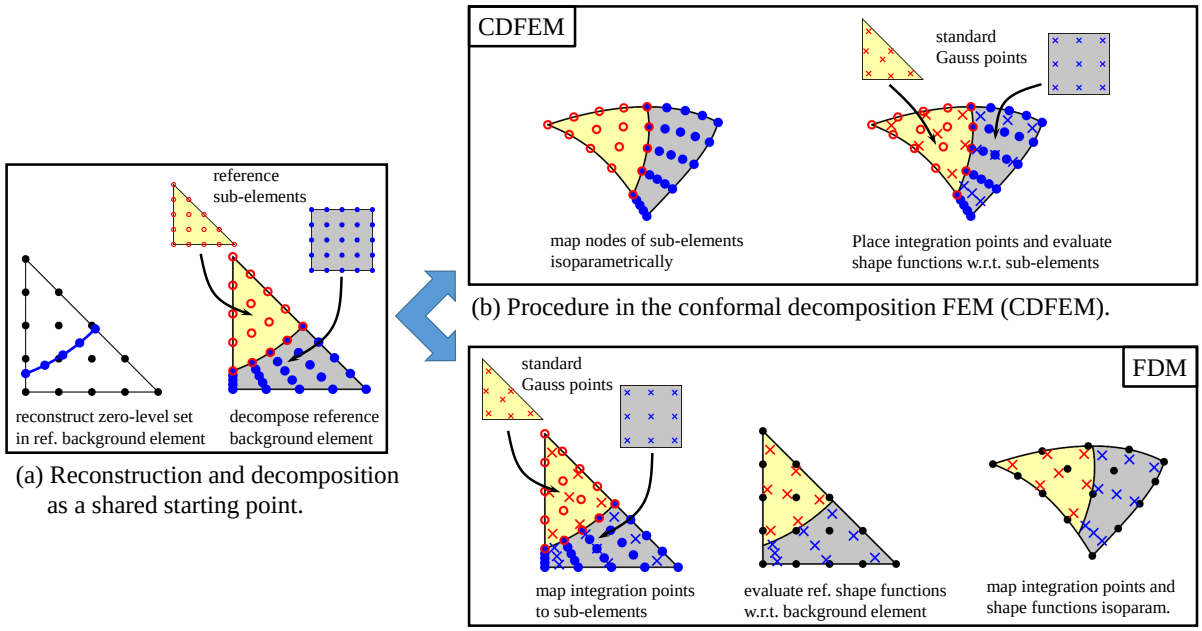

(a) Reconstruction and decomposition as a shared starting point.

(b) Procedure in the conformal decomposition FEM (CDFEM).

(c) Procedure in the fictitious domain method (FDM).

Figure 2: Schematic overview of the procedure: (a) The shared starting point is the reconstruction and decomposition of the reference background elements. (b) In the CDFEM, the sub-elements are mapped to the physical background element and treated as standard finite elements. (c) In the FDM, the sub-elements are only needed in the reference background elements to place integration points. Then shape functions of the background nodes are evaluated and mapped to the physical domain.

3 CONFORMAL DECOMPOSITION FINITE ELEMENT METHOD (CDFEM)

In the CDFEM, the task is to generate a *regular*, higher-order mesh composed by the (sub-)elements that conform to all zero-level sets and are part of the domain of interest Ω. Therefore, the resulting sub-elements in the *reference* background elements from step 4 (see above) are mapped to the physical domain, see Fig. 2(b). By "regular" mesh, we refer to the desired property not to allow hanging nodes which, otherwise, would require additional measures in the context of FE analyses. This is naturally achieved only provided that (i) the background mesh is regular and (ii) *all* decompositions (in the background elements) are successful.

However, the decomposition described above may fail in elements where (a) the level-set data is too complex to obtain valid topological cut situations, (b) the identified nodes on the zero-level set are outside the element, or (c) the Jacobian of a decomposed sub-element (in the reference or physical background element) may be negative, hence, invalid. Then, the background mesh is adaptively refined until the decomposition is successful. The regularity of the background mesh, i.e., the absence of hanging nodes must be ensured because this, in turn, also ensures the regularity of the resulting conforming mesh. That is, the failure to decompose a certain background element requires an adaptive refinement of this element also affecting neighbor elements to avoid hanging nodes. Adaptivity may

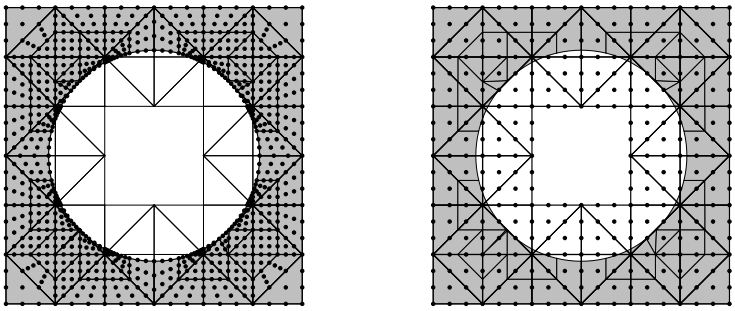

(a) Mesh for CDFEM (b) Mesh for FDM

Figure 3: Resulting example meshes (of order 3) used for the (a) CDFEM and (b) FDM for the example of a plate with hole.

also be useful to better resolve geometry features or improve the approximations. The interplay between decomposition and adaptivity is further outlined in [11].

It is thus found that the overall decomposition of the background mesh with respect to all level-set functions, leading to a regular, conforming mesh of sub-elements is a major implementational challenge. Of course, the advantage is that, once successful, such a mesh is used as in classical p-FEM analyses. It is noted that the resulting meshes are mixed in the sense that they feature triangular and quadrilateral elements in one mesh. If this is undesired, one may easily convert them to meshes composed by one element type only. Furthermore, it is mentioned that to avoid ill-shaped elements, it is recommended to (slightly) modify the nodes of the underlying background mesh such that they are not too close to the zero-level sets which is outlined in [14, 23]. Fig. 3(a) shows an automatically generated, conforming mesh for the CDFEM for the example of a plate with hole.

4 FICTITIOUS DOMAIN METHOD (FDM)

The decomposition in the reference background elements according to Section 2 is also needed for the FDM. Then, based on these sub-cells, integration points are mapped to the reference background elements and the background shape functions are evaluated there, see Fig. 2(c). Integration points and shape functions are mapped to the physical background elements. In order to improve the conditioning of the resulting system of equations, it is useful to consider a "virtual" material inside the void regions with a negligible Young's modulus $E^\star$ following [8, 26, 30].

In order to consider boundary conditions (weakly), Lagrange multipliers or the penalty method is employed. Therefore, an integration along the corresponding boundary segments is required (falling into Dirichlet and Neumann parts). This is trivial in the CDFEM as it is the same than in classical FEM analyses. In the FDM, it is found useful to have the full CDFEM-mesh available because—in addition to defining the integration sub-cells—this naturally represents a *discretization* of the boundary which is, for the FDM, within elements. For enforcing the constraints in the FDM one has to (i) integrate along the element boundaries of the CDFEM-mesh, (ii) evaluate the lower-dimensional CDFEM-shape functions on the trace of the boundary, and (iii) evaluate shape functions

of the background mesh.

5 NUMERICAL RESULTS

Applications in linear elasticity are considered herein. The corresponding governing equations are found in many text books, e.g., [2, 35]. These equations are not repeated here and also the formal enforcement of boundary conditions via Lagrange multipliers or the penalty method can be considered standard.

The test cases considered herein follow those presented in [11] where further details are found. The test cases either feature analytical solutions or overkill approximations have been generated to extract benchmark quantities such as the stored elastic energy. In the first case, errors are measured in the L_2-norm of the displacements, $\varepsilon_{\boldsymbol{u}}$, and in the second, the convergence of the stored elastic energy to the benchmark result is observed, $\varepsilon_\Pi = \Pi^h - \Pi^{\text{overkill}}$. The condition numbers $\varkappa$ are computed using Matlab's condest-function. The negligibly small Young's modulus prescribed in void regions is labelled $E^\star$ implying some "virtual" material.

5.1 Square shell with circular hole

A square shell with dimensions $[-1,1]\times[-1,1]$ is considered with a circular void region of radius $R = 0.7123$. Plane strain conditions are assumed with Young's modulus $E = 1000$ and Poisson's ratio $\nu = 0.3$. The exact solution is found in [32, 18, 6]. The corresponding displacements are prescribed along the outer boundary of the domain, the inner boundary to the void is traction-free. Because the outer boundary is conforming in the CDFEM just as for the FDM, see Fig. 3, nodal values may be directly prescribed without using Lagrange multipliers or the penalty method. Background meshes in $[-1,1]\times[-1,1]$ with quadrilateral and triangular elements of different orders are considered. For the convergence study, the number of elements, n_d, per dimension of the background mesh is systematically increased and $n_d = \{6, 10, 20, 30, 50, 70, 100\}$ elements are used with varying orders between 1 and 6.

Results are shown in Fig. 4. The upper sub-figures show the approximation errors $\varepsilon_{\boldsymbol{u}}$ and the lower sub-figures the corresponding condition numbers $\varkappa$. It is seen in Figs. 4(a) and (d) for triangular elements that when the void region is completely neglected ($E^\star = 0$), $\varkappa$ is very high but, nevertheless, optimal convergence rates are achieved. For quadrilateral elements in Figs. 4(b) and (e), $\varkappa$ is even worse and convergence rates are disturbed for elements with higher order than 3. Therefore, it is useful to assign the virtual Young's modulus $E^\star = 10^{-7}$ to the void region: As can be seen in Figs. 4(c) and (f), this clearly bounds $\varkappa$ and still enables optimal convergence rates up to $\varepsilon \approx 10^{-9}$. The effect of $E^\star$ on $\varepsilon_{\boldsymbol{u}}$ and $\varkappa$ is further investigated in Fig. 5. Obviously, $\varkappa$ is better for higher $E^\star$ but $\varepsilon_{\boldsymbol{u}}$ is better for lower $E^\star$. As long as direct solvers are employed, already very small values for $E^\star$ are acceptable for the conditioning and yield very accurate results. It is noted that the results for the CDFEM are found in [11]: Optimal convergence rates are achieved there with significantly smaller condition numbers than for the FDM (with $E^\star = 0$).

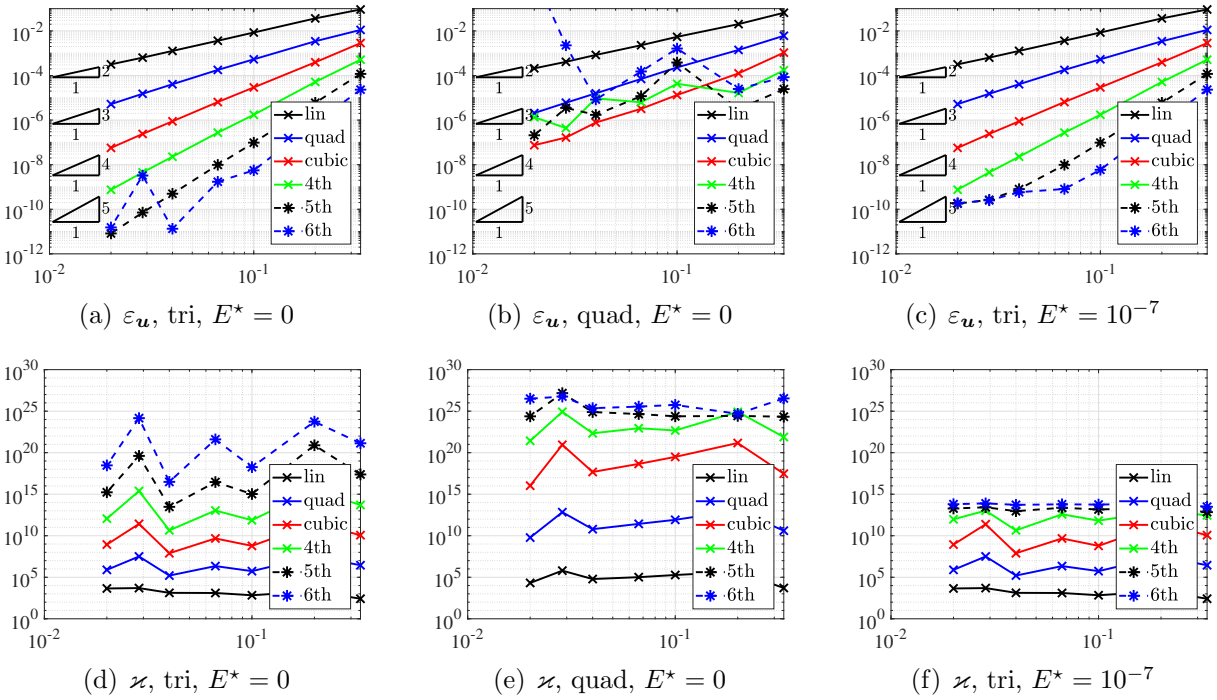

(a) $\varepsilon_{\boldsymbol{u}}$, tri, $E^\star = 0$ (b) $\varepsilon_{\boldsymbol{u}}$, quad, $E^\star = 0$ (c) $\varepsilon_{\boldsymbol{u}}$, tri, $E^\star = 10^{-7}$

(d) $\varkappa$, tri, $E^\star = 0$ (e) $\varkappa$, quad, $E^\star = 0$ (f) $\varkappa$, tri, $E^\star = 10^{-7}$

Figure 4: Plate with hole test case: (a), (b), and (c) show approximation errors $\varepsilon_{\boldsymbol{u}}$, (d), (e), and (f) the corresponding condition numbers $\varkappa$.

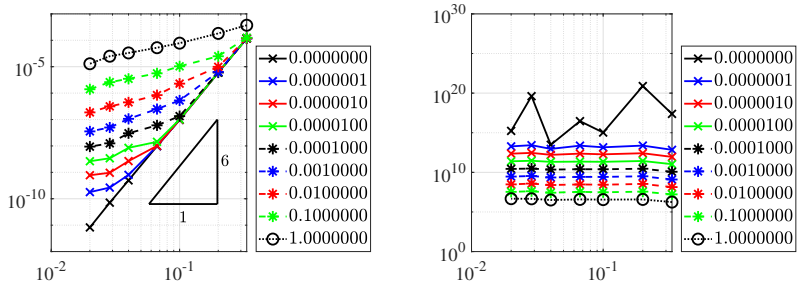

(a) $\varepsilon_{\boldsymbol{u}}$ for various $E^\star$ (b) $\varkappa$ for various $E^\star$

Figure 5: Plate with hole test case: (a) approximation errors $\varepsilon_{\boldsymbol{u}}$, and (b) condition numbers $\varkappa$ for 5th-order triangular elements and various values for the virtual Young's modulus $E^\star$ inside the hole.

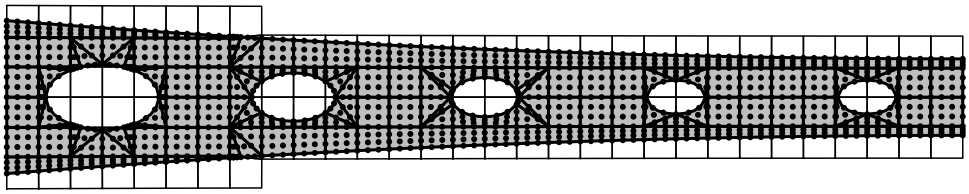

(a) Mesh for CDFEM

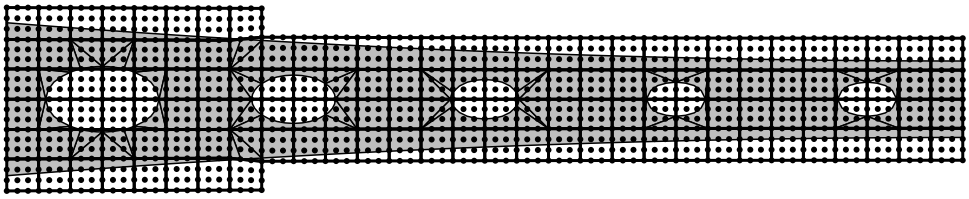

(b) Mesh for FDM

Figure 6: Cantilever beam: example meshes (of order 3) for the (a) CDFEM and (b) FDM.

5.2 Cantilever beam

A cantilever beam with length $L = 5.0\,\mathrm{m}$ and a variable thickness between $h = 0.2\,\mathrm{m}$ and $0.4\,\mathrm{m}$ is considered. The beam features several elliptical voids and the detailed geometry definition is given in [11], see Fig. 6 for the domain and example meshes used in the CDFEM and FDM. The material is composed of steel with $E = 2.1 \cdot 10^8\,\mathrm{kN/m^2}$ and $\nu = 0.3$. The beam is loaded by gravity acting as a body force of $f_y = -78.5\,\mathrm{kN/m^3}$ and a vertical traction on the right end. This traction is distributed in a quadratic profile being zero at the upper and lower right side and reaching a maximum of $\sigma_y = -100\,\mathrm{kN/m}$ in between, leading to a force resultant of $F_y = -26.\bar{6}\,\mathrm{kN}$. The beam is fixed along the boundary of the left elliptical hole leading to smooth solutions and enabling higher-order convergence rates. The Lagrange multiplier method yields extremely high condition numbers wherefore we prefer the penalty method here. The stored elastic energy may be determined by an overkill solution and is $\Pi^{\mathrm{overkill}} = 0.02361112384 \pm 10^{-10}\,\mathrm{kNm}$. Convergence results are shown in Fig. 7 using $E^\star = 0.01$: Higher-order convergence rates are found and the condition numbers are bounded as expected. For this more advanced geometry, the convergence curves are not as smooth as for the previous test case.

5.3 Spanner

Next, the geometry shown in Fig. 8 is considered and refers to a spanner being very similar to normed spanner geometries defined in DIN 895. The geometry is embedded into a universal mesh composed by triangular elements of different orders. 11 level-set functions are employed to define the geometry, see [11] for the detailed definitions. The material is again composed by steel with $E = 2.1 \cdot 10^5\,\mathrm{N/mm^2}$ and $\nu = 0.3$. The beam is loaded by gravity acting as a body force of $f_y = -78.5 \cdot 10^{-6}\,\mathrm{N/mm^3}$ and a traction at the end of the handle. This traction acts in parallel direction of the handle and is distributed linearly between $-100\mathrm{N/mm}$ at the bottom side and $+100\,\mathrm{N/mm}$ on the top side. It loads the handle of the spanner with a resulting bending moment of $M_z = 38400\,\mathrm{Nmm}$. All

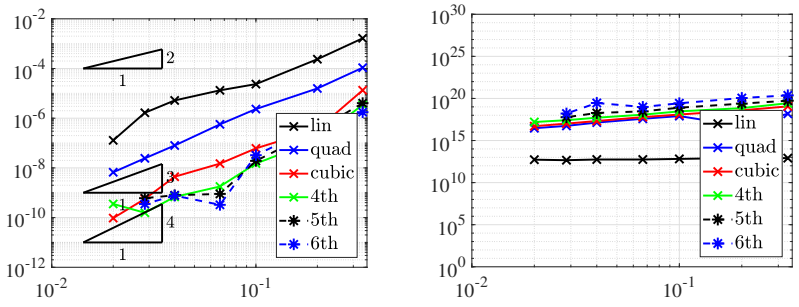

(a) ε_Π (b) $\varkappa$

Figure 7: Cantilever test case: (a) stored energy errors ε_Π, and (b) condition numbers $\varkappa$ for $E^\star = 0.01$ and the penalty method with $\alpha = 10^{18}$.

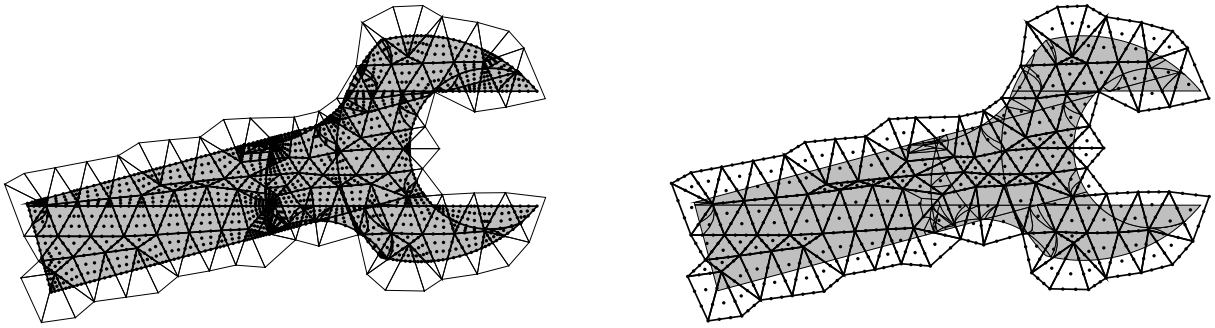

(a) Mesh for CDFEM (b) Mesh for FDM

Figure 8: Spanner: example meshes (of order 3) for the (a) CDFEM and (b) FDM.

nodes on the two straight, parallel sides of the mouth are fixed. It is clear that singular stresses have to be expected at all reentrant corners so that only first order convergence rates may be expected for this test case. Again, there is no analytical solution available wherefore the stored energy is used for the convergence study. An overkill solution yields $\Pi^{\text{overkill}} = 61.49248 \pm 10^{-4}\,\text{Nmm}$. Fig. 9 shows convergence results in ε_Π and condition numbers using the penalty method with $\alpha = 10^{12}$. The fictitious Young's modulus $E^\star$ is set to 1.0 and the expected convergence rates are obtained. Results for the CDFEM are presented in [11].

6 CONCLUSIONS

A fictitious domain method is presented which is based on the accurate integration in elements cut by (multiple) zero-level sets. This is achieved by generating conforming higher-order sub-elements (through reconstruction and decomposition in cut elements) which are used as integration cells in the FDM. In an alternative method called CDFEM, these sub-elements rather play the role of typical finite elements and imply basis functions. In the FDM presented, boundary conditions are enforced preferably by the penalty method which turned out to be more robust than using Lagrange multipliers. Conditioning issues are addressed by assigning a virtual material in the void regions with negligible material

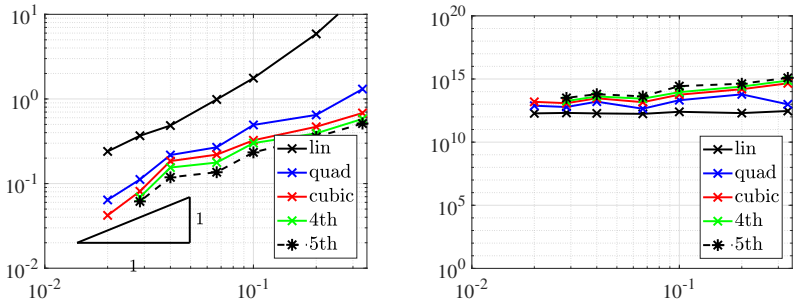

(a) ε_Π (b) $\varkappa$

Figure 9: Spanner test case: (a) stored energy errors ε_Π, and (b) condition numbers $\varkappa$ for $E^\star = 1.0$ and the penalty method with $\alpha = 10^{12}$.

parameters.

We find that using the virtual material in void regions in combination with the penalty method possibly yields the most simple version of a FDM. Although it is found that higher-order convergence rates can be achieved with this simplistic setting, it is more consistent to enforce (i) boundary conditions based on Nitsche's method and (ii) solve conditioning issues by stabilization. The resulting FDM is then basically a CutFEM [4, 5, 3, 15] which shall be combined with our higher-order accurate integration schemes in future works.

REFERENCES

[1] Abedian, A.; Parvizian, J.; Düster, A.; Rank, E.: The finite cell method for the J_2 flow theory of plasticity. *Finite Elem. Anal. Des.*, **69**, 37–47, 2013.

[2] Belytschko, T.; Liu, W.K.; Moran, B.: *Nonlinear Finite Elements for Continua and Structures*. John Wiley & Sons, Chichester, 2000.

[3] Burman, E.; Claus, S.; Hansbo, P.; Larson, M.G.; Massing, A.: CutFEM: Discretizing geometry and partial differential equations. *Internat. J. Numer. Methods Engrg.*, **104**, 472–501, 2015.

[4] Burman, E.; Hansbo, P.: Fictitious domain finite element methods using cut elements: I. A stabilized Lagrange multiplier method. *Comp. Methods Appl. Mech. Engrg.*, **199**, 2680–2686, 2010.

[5] Burman, E.; Hansbo, P.: Fictitious domain finite element methods using cut elements: II. A stabilized Nitsche method. *Applied Numerical Mathematics*, **62**, 328–341, 2012.

[6] Cheng, K.W.; Fries, T.P.: Higher-order XFEM for curved strong and weak discontinuities. *Internat. J. Numer. Methods Engrg.*, **82**, 564–590, 2010.

[7] Cottrell, J.A.; Hughes, T.J.R.; Bazilevs, Y.: *Isogeometric Analysis*. John Wiley & Sons, Chichester, 2009.

[8] Düster, A.; Parvizian, J.; Yang, Z.; Rank, E.: The finite cell method for three-dimensional problems of solid mechanics. *Comp. Methods Appl. Mech. Engrg.*, **197**, 3768–3782, 2008.

[9] Fries, T.P.: Higher-order accurate integration for cut elements with Chen-Babuška nodes. In *Advances in Discretization Methods: Discontinuities, virtual elements, fictitious domain methods*. (Ventura, G.; Benvenuti, E., Eds.), Vol. 12, *SEMA SIMAI Springer Series*, Springer, Berlin, 245–269, 2016.

[10] Fries, T.P.: Higher-order meshing of implicit geometries—part III: Conformal decomposition FEM (CDFEM). *arXiv: 1706.00919*, 2017.

[11] Fries, T.P.: Higher-order Conformal Decomposition FEM (CDFEM). *Comp. Methods Appl. Mech. Engrg.*, **328**, 75–98, 2018.

[12] Fries, T.P.; Omerović, S.: Higher-order accurate integration of implicit geometries. *Internat. J. Numer. Methods Engrg.*, **106**, 323–371, 2016.

[13] Fries, T.P.; Omerović, S.; Schöllhammer, D.; Steidl, J.: Higher-order meshing of implicit geometries—part I: Integration and interpolation in cut elements. *Comp. Methods Appl. Mech. Engrg.*, **313**, 759–784, 2017.

[14] Fries, T.P.; Schöllhammer, D.: Higher-order meshing of implicit geometries—part II: Approximations on manifolds. *Comp. Methods Appl. Mech. Engrg.*, **326**, 270–297, 2017.

[15] Hansbo, A.; Hansbo, P.: An unfitted finite element method, based on Nitsche's method, for elliptic interface problems. *Comp. Methods Appl. Mech. Engrg.*, **191**, 5537–5552, 2002.

[16] Kramer, R.M.J.; Noble, D.R.: An effective strategy for improving the quality of conformal mesh decompositions on unstructured simplex meshes. *Internat. J. Numer. Methods Engrg.*, **0**, submitted, 2017.

[17] Leveque, R.; Randall, J.; Li, Z.: Immersed interface method for elliptic equations with discontinuous coefficients and singular sources. *SIAM J. Numer. Anal.*, **31**, 1019–1044, 1994.

[18] Liu, G.R.: *Meshless Methods*. CRC Press, Boca Raton, 2002.

[19] Loehnert, S.: A stabilization technique for the regularization of nearly singular extended finite elements. *Comput. Mech.*, **54**, 523–533, 2014.

[20] Löhner, R.; Cebral, J.R.; Camelli, F.F.; Baum, J.D.; Mestreau, E.L.; Soto, O.A.: Adaptive embedded/immersed unstructured grid techniques. *Archives Of Computational Methods In Engineering*, **14**, 279–301, 2007.

[21] Neittaanmäki, P.; Tiba, D.: An embedding of domains approach in free boundary problems and optimal design. *SIAM J. Control Optim.*, **33**, 1587–1602, 1995.

[22] Noble, D.R.; Newren, E.P.; Lechman, J.B.: A conformal decomposition finite element method for modeling stationary fluid interface problems. *Int. J. Numer. Methods Fluids*, **63**, 725–742, 2010.

[23] Omerović, S.; Fries, T.P.: Conformal higher-order remeshing schemes for implicitly defined interface problems. *Internat. J. Numer. Methods Engrg.*, **109**, 763–789, 2017.

[24] Osher, S.; Fedkiw, R.P.: Level set methods: an overview and some recent results. *J. Comput. Phys.*, **169**, 463–502, 2001.

[25] Osher, S.; Fedkiw, R.P.: *Level Set Methods and Dynamic Implicit Surfaces*. Springer, Berlin, 2003.

[26] Parvizian, J.; Düster, A.; Rank, E.: Finite cell method: h- and p-extension for embedded domain problems in solid mechanics. *Comput. Mech.*, **41**, 121–133, 2007.

[27] Piegl, L.; Tiller, W.: *The NURBS Book (Monographs in Visual Communication)*. Springer, Berlin, 2 edition, 1997.

[28] Saiki, E.M.; Biringen, S.: Numerical Simulation of a Cylinder in Uniform Flow: Application of a Virtual Boundary Method. *J. Comput. Phys.*, **123**, 450–465, 1996.

[29] Schillinger, D.; Düster, A.; Rank, E.: The *hp-d*-adaptive finite cell method for geometrically nonlinear problems of solid mechanics. *Internat. J. Numer. Methods Engrg.*, **89**, 1171–1202, 2012.

[30] Schillinger, D.; Ruess, M.: The Finite Cell Method: A Review in the Context of Higher-Order Structural Analysis of CAD and Image-Based Geometric Models. *Archive Comp. Mech. Engrg.*, **22**, 391–455, 2015.

[31] Sethian, J.A.: *Level Set Methods and Fast Marching Methods*. Cambridge University Press, Cambridge, 2 edition, 1999.

[32] Szabó, B.; Babuška, I.: *Finite Element Analysis*. John Wiley & Sons, Chichester, 1991.

[33] Uzgoren, E.; Sim, J.; Shyy, W.: Marker-based, 3-D adaptive Cartesian grid method for multiphase flow around irregular geometries. *Comput. Phys. Comm.*, **5**, 1–41, 2009.

[34] Ye, T.; Mittal, R.; Udaykumar, H.S.; Shyy, W.: An Accurate Cartesian Grid Method for Viscous Incompressible Flows with Complex Immersed Boundaries. *J. Comput. Phys.*, **156**, 209–240, 1999.

[35] Zienkiewicz, O.C.; Taylor, R.L.: *The Finite Element Method*, Vol. 1-3. Butterworth-Heinemann, Oxford, 2000.